Hindawi
Advances in Mathematical Physics
Volume 2022, Article ID 1637071, 15 pages
https://doi.org/10.1155/2022/1637071

Research Article

Pulse Dynamics in a Bistable Reaction-Diffusion System with Chemotaxis

Satoshi Kawaguchi

Department of Complex and Intelligent Systems, School of Systems Information Science, Future University Hakodate, Hakodate 041-8655, Japan

Correspondence should be addressed to Satoshi Kawaguchi; satoshi@fun.ac.jp

Received 23 May 2022; Revised 27 July 2022; Accepted 29 July 2022; Published 12 September 2022

Academic Editor: Kang-Jia Wang

We consider pulse dynamics in a bistable reaction-diffusion system with chemotaxis. We derive the ordinary differential equation of interfaces by applying the multiple scales method to the reaction-diffusion system for examining the effect of the chemotaxis on pulse dynamics in one dimension. The stability of the standing pulse is considered by two different methods, and the applicability of the methods is demonstrated. The chemotaxis influences the Hopf and drift bifurcations and the collision of two traveling pulses. It also enlarges the bifurcation point and enhances the repulsive force between pulses so that the parameter region of the elastic collision becomes large. Although the ordinary differential equation of interfaces can describe the elastic collision, it cannot describe the pair annihilation of pulses caused by the collision. The conditions for the reliable calculation of pulse collision are discussed.

1. Introduction

Reaction-diffusion (RD) systems are employed in wide fields. The normal diffusion equation, which underlies the Brownian motion of particles, is derived by using the equation of continuity (law of conservation of mass) and Fick's law. Although the mean squared displacement (MSD) of particles is linear in time for the normal diffusion, there are cases where the MSD is described by a power law [1]. For these cases, the anomalous diffusion is modeled using fractional or fractal derivatives, where the usual second derivative in space is replaced by a fractional derivative of order $0 < \alpha < 2$ [2, 3]. The fractional derivative is employed in many fields such as control engineering, condensed matter physics, and electronics. For example, the vibration of viscoelastic bodies, thermal conduction in amorphous semiconductors, and discharge of Lithium-ion batteries are studied. On the other hand, the fractal derivative is introduced on the basis of the fractal concept to model power law scaling phenomena such as the turbulence, seepage in porous media, and groundwater flow in aquifer [4, 5]. Although it is almost impossible to obtain an analytic solution of anomalous diffusion systems, methods to solve them have been proposed such as the variational approach [6], homotopy perturbation method [7], and reproducing kernel method [8]. By contrast, with the use of normal diffusion, many RD systems have been proposed to describe the spatiotemporal patterns in physics, chemistry, biology, and neuroscience [9–12]. A homogeneous state is destabilized through the Turing instability, resulting in inhomogeneous states such as front and pulse [13].

The pulse dynamics and motion of interfaces have been considered in many systems [14–17]. For example, center manifold reduction with a weak interaction theory is employed in RD systems when front or pulse solutions of the system interact weakly [18–21]. Additionally, Kusaka derived the equation of motion of interfaces, that is, the ordinary differential equation (ODE) system by applying the method to a bistable RD system [22]. However, significant differences were observed when comparing the numerical results obtained using the RD system with that obtained using the ODE system. In the RD system, the standing pulse was destabilized through the Hopf bifurcation by changing a bifurcation parameter, and this was

followed by drift bifurcation. By contrast, in the ODE system, the order of the bifurcation was reversed. Nishi et al. applied the multiple scales method to the RD system to overcome this discrepancy [23]. The multiple scales method has been employed to examine the bifurcatoin of a stationary solution in many systems [24–26]. By applying the multiple scales method to the bistable RD system, an extra term was added in addition to the equations obtained by Kusaka in ref. [22]; this term corrected the above discrepancy. However, the stability analysis of the ODE system did not agree well with the numerical simulation results. Therefore, the ODE system was reliable only within a limited parameter region.

Chemotaxis is an important mechanism for moving and transporting biological substances in biology [27, 28]. Living organisms efficiently utilize chemotaxis to survive in an external environment [29, 30]. The process of chemotaxis involves the detection of the direction of the gradient of the chemical substances in two or three dimensions in a biological organ; after the chemotactic substance is detected, the cell moves to or away from the source depending on whether the substances are chemoattractant or chemorepellent, respectively [31, 32]. Chemotaxis is proportional to the gradient of the chemical substance in the medium. The mathematical model of chemotaxis was proposed by Keller and Segel, wherein the flow of amoeba was modeled by the gradient of the chemoattractant [33, 34]. The collective movement of bacteria caused by chemotaxis has been observed and modeled based on the Keller-Segel model [35–39]. Recently, pulse-shaped bacterial colonies, which traveled along one direction, have been observed [32, 40–42]. Additionally, two types of collision of the pulse-shaped bacterial colonies were considered in a model under experimental conditions [43]. Although the mathematical models of traveling waves were considered, the stability and bifurcation of the solution were not sufficiently explained [44, 45]. Even if the stability and bifurcation of the spatially uniform state were considered in ref. [46], the traveling pulse did not exist in their model.

To clarify the mechanism of emergence of bacterial traveling pulse, it is necessary to examine the stability of the stationary pulse in a mathematically tractable model. Thus, in this study, we consider the pulse dynamics in a bistable RD system with chemotaxis. Following ref. [23], we employ the multiple scales method for the model and derive an ODE system. First, we consider the stability of the standing pulse to examine the effect of chemotaxis on the system. Then, we consider the collision of two traveling pulses and compare the mechanisms of the repulsion of pulses observed in other models. Finally, reliable conditions of traveling pulse and pulse collision in the ODE system are discussed.

2. RD System and Reduced ODE System without Chemotaxis

In this section, we introduce the preceding study reported in ref. [23] and briefly explain the properties of the bistable RD and ODE systems. A two-component RD system without chemotaxis in one dimension was proposed [21, 22]. Activator u and inhibitor v satisfy the time evolution equation:

$$\begin{aligned}\tau\varepsilon\frac{\partial u}{\partial t} &= \varepsilon^2\frac{\partial^2 u}{\partial x^2} + f(u,v),\\ \frac{\partial v}{\partial t} &= D\frac{\partial^2 v}{\partial x^2} + g(u,v),\end{aligned} \tag{1}$$

with

$$\begin{aligned}f(u,v) &= \left(u+\frac{1}{2}\right)\left(\frac{1}{2}-u\right)\left(u-\frac{1}{2}v\right),\\ g(u,v) &= u - v + \theta_0,\end{aligned} \tag{2}$$

where we choose ε and θ_0 such that $0 < \varepsilon \ll 1$ and $0 \le \theta_0 \le 1/2$. Here, τ and D represent the positive constants.

Let us briefly summarize the solution of system (1). When $\theta_0 = 0$, system (1) has stationary front solutions connecting $u = \pm 1/2$ for a large τ. The stationary front solution bifurcates to the traveling front solutions when τ is decreased to less than the critical value τ_c. However, system (1) does not have a pulse solution because of the odd symmetry of the reaction terms $f(u,v)$ and $g(u,v)$. For $\theta_0 > 0$, the odd symmetry is broken, and system (1) has pulse solutions. The pulse solution is called the front-back pulse because the system is bistable; the pulse is caught by two interfaces that connect two stable points. There are four types of solutions depending on the value of τ: standing pulse, standing breather, traveling breather, and traveling pulse.

The velocity of the interface is obtained as $\pm v_i/(\tau\sqrt{2})$, where v_i corresponds to the value of v at the interface [47]. The equations of motion of the left and right interfaces were derived by applying the multiple scales method to Equation (1) [23]. We consider one pulse in system (1) and denote the positions of the left and right interfaces of the pulse as $l_1(t)$ and $l_2(t)$, respectively. The equations of motion of l_1 and l_2 are

$$\begin{aligned}\dot{l}_1 &= r_1,\\ \dot{l}_2 &= r_2,\\ m_0\dot{r}_1 &= \sqrt{2}(\tau_c-\tau)r_1 - g_3 r_1^3\\ &\quad - (G_0 + G_1 r_2)e^{-(-r_2+\phi(r_2))h/(2D)} + \theta_0,\\ m_0\dot{r}_2 &= \sqrt{2}(\tau_c-\tau)r_2 - g_3 r_2^3\\ &\quad + (G_0 - G_1 r_1)e^{-(r_1+\phi(r_1))h/(2D)} - \theta_0,\end{aligned} \tag{3}$$

where overdot $\dot{l}$ denotes the time derivative of variable $l(t)$, $\phi(r)=\sqrt{r^2+4D}$, and pulse width $h=l_2-l_1$ ($l_2>l_1$). The parameters in Equation (3) are $m_0 = 3/(16\sqrt{D})$, $\tau_c = 1/(4\sqrt{2D})$, $g_3 = 1/(32(\sqrt{D})^3)$, $G_0 = 1/2$, and $G_1 = 1/(4\sqrt{D})$. System (3) is called the reduced ODE system. The inhibitor v causes repulsive interaction between pulses. The

reduced ODE system (3) is valid for $|\tau - \tau_c| \ll 1$, $0 < \theta_0 < 1/2$, $|r_1|$, $|r_2| \ll 1$, and $h \gg 1$.

The linear stability of the stationary state, $r_1 = r_2 = 0$ with a pulse width $h_0 = -\sqrt{D}\log(2\theta_0)$, was studied [23]. Although the standing pulse was stable for a large τ, it was destabilized through the Hopf bifurcation as τ decreased at $\tau_H = \tau_c + \sqrt{2}\theta_0(G_1 + G_0 h_0/(2D))$, and a standing breather appeared. The standing breather was destabilized through pitchfork bifurcation with a further decrease in τ; then, the standing breather started to move while retaining interface oscillation (i.e., a traveling breather). With a further decrease in τ, the interface oscillation ceased, and the traveling breather changed to a traveling pulse at $\tau_d = \tau_c - \sqrt{2}\theta_0 (G_1 + G_0 h_0/(2D))$. There exists a small parameter region of coexistence between the standing and traveling breathers. Although the bifurcation points are obtained by the RD, and reduced ODE systems agreed well for small values of θ_0 with $|\tau - \tau_c| \ll 1$, the bifurcation points obtained by the two methods were different for larger values of θ_0.

3. RD System and Reduced ODE System with Chemotaxis

We now consider a two-component RD system with chemotaxis in one dimension. We denote the population density of biological individuals and concentration of chemotactic substance by u and v, respectively. We assume the case wherein the chemotactic substance is released from the biological individual, and it diffuses outward and influences the movement of each individual. We consider the following time evolution equations of u and v:

$$\begin{aligned} \tau\varepsilon\frac{\partial u}{\partial t} &= \varepsilon^2\frac{\partial^2 u}{\partial x^2} - \varepsilon\frac{\partial}{\partial x}\left(u\frac{\partial \chi(v)}{\partial x}\right) + f(u,v), \\ \frac{\partial v}{\partial t} &= D\frac{\partial^2 v}{\partial x^2} + g(u,v), \end{aligned} \tag{4}$$

where f and g are the same as Equation (2); χ corresponds to the chemotactic sensitivity function given by $\chi(v) = k_c f_0 v^2 a/(v^2 + a^2)$. For $a = 1$, we choose f_0 such that the condition $\max|df_0 v^2 a/(v^2 + a^2)/dv| = 1$ is satisfied; $f_0 = 8\sqrt{3}/9$. k_c (≥ 0) represents the intensity of the chemotaxis [48]. We choose ε and θ_0 such that $0 < \varepsilon \ll 1$ and $0 \leq \theta_0 \leq 1/2$. Here, τ and D represent positive constants. We note three important points about system (4). First, because we use $f(u,v)$ and $g(u,v)$ as presented in Equation (2), the ranges of u and v are $-1/2 \leq u, v \leq 1/2$. From the practical perspective, the population density of biological individuals u and concentration of chemotactic substance v should satisfy $u, v \geq 0$. To overcome this problem, although we adopt system (4) in the calculation, the values u and v shall be replaced with $(u + 1/2)$ and $(v + 1/2)$, respectively, in practical situations (experiments). Second, v represents not only the concentration of chemotactic substance but also the concentration of inhibitor in system (4). This dual role of v is a new aspect of the system. Third, we note the difference between our model (4) and other chemotaxis models [40, 41, 43]. In these models, three variables are introduced: the density of bacteria, concentration of cheomotactic substance, and concentration of nutrition. In our model, the variable of the concentration of nutrition is not considered; it corresponds to the scenario that the nutrition is sufficiently supplied, and therefore, we do not need to consider its distribution. In this study, we consider the effect of the chemotaxis on the pulse solution. The dual role of v as the chemotactic substance and inhibitor changes the stability of the standing pulse, and it reduces the velocity of pulses during the collision. We consider the stabilty of the standing pulse solution by two different methods: the singular perturbation method of the interface and the linear stability of the reduced ODE system. Further, we consider the collision of the two traveling pulses. Then, we compare the numerical results obtained by the direct calculation of the RD and reduced ODE systems to obtain reliable conditions for the reduced ODE system.

3.1. Reduced ODE System of One Pulse. In the presence of chemotaxis, the equation of motion of interface is given ([31, 36, 47]) by

$$\begin{aligned} \frac{dl_1}{dt} &= \frac{1}{\tau}\left[\frac{v(l_1)}{\sqrt{2}} + k_c\frac{2f_0 a^3 v(l_1)}{\left(v(l_1)^2 + a^2\right)^2}\left(\frac{dv}{dx}\right)\Big|_{x=l_1}\right], \\ \frac{dl_2}{dt} &= \frac{1}{\tau}\left[-\frac{v(l_2)}{\sqrt{2}} + k_c\frac{2f_0 a^3 v(l_2)}{\left(v(l_2)^2 + a^2\right)^2}\left(\frac{dv}{dx}\right)\Big|_{x=l_2}\right]. \end{aligned} \tag{5}$$

Thus, it is determined by the values of v and (dv/dx) at the interface. Following the process reported in ref. [23], we derive the reduced ODE system of the RD system with chemotaxis. The brief derivation is given in Appendix A. The equations of motion of interface have the same form as in Equation (3); however, the parameters are different. The final expressions are

$$\begin{aligned} \dot{l}_1 &= r_1, \\ \dot{l}_2 &= r_2, \\ m_0\dot{r}_1 &= \sqrt{2}(\tau_c - \tau)r_1 - g_3 r_1^3 \\ &\quad - (G_0 + G_1 r_2)e^{-(-r_2 + \phi(r_2))h/(2D)} + \Delta_0, \\ m_0\dot{r}_2 &= \sqrt{2}(\tau_c - \tau)r_2 - g_3 r_2^3 \\ &\quad + (G_0 - G_1 r_1)e^{-(r_1 + \phi(r_1))h/(2D)} - \Delta_0, \end{aligned} \tag{6}$$

where the parameters are

$$\begin{aligned} m_0 &= \frac{3}{16\sqrt{D}} + \left(\frac{2f_0 k_c}{a}\right)\frac{3\sqrt{2}}{32D}, \\ \tau_c &= \frac{1}{4\sqrt{2D}} + \left(\frac{2f_0 k_c}{a}\right)\frac{(1 - 2\theta_0)}{8D}, \end{aligned}$$

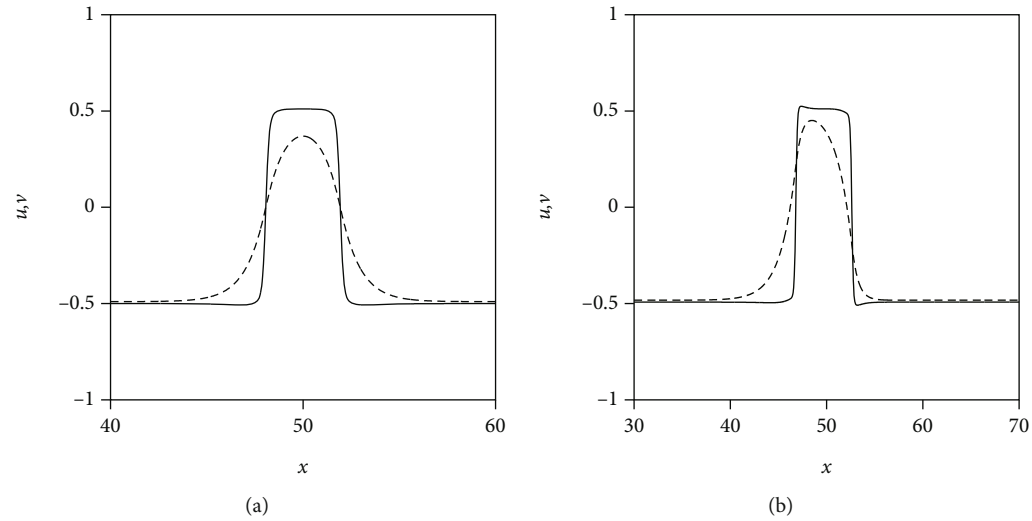

Figure 1: Profiles of standing and traveling pulses in the RD system (4). Solid and dashed curves represent u and v, respectively. System size $L = 100$, $k_c = 1$, and $\theta_0 = 1 \times 10^{-2}$. (a) Standing pulse. $\tau = 0.6$. (b) Traveling pulse. $\tau = 0.4$.

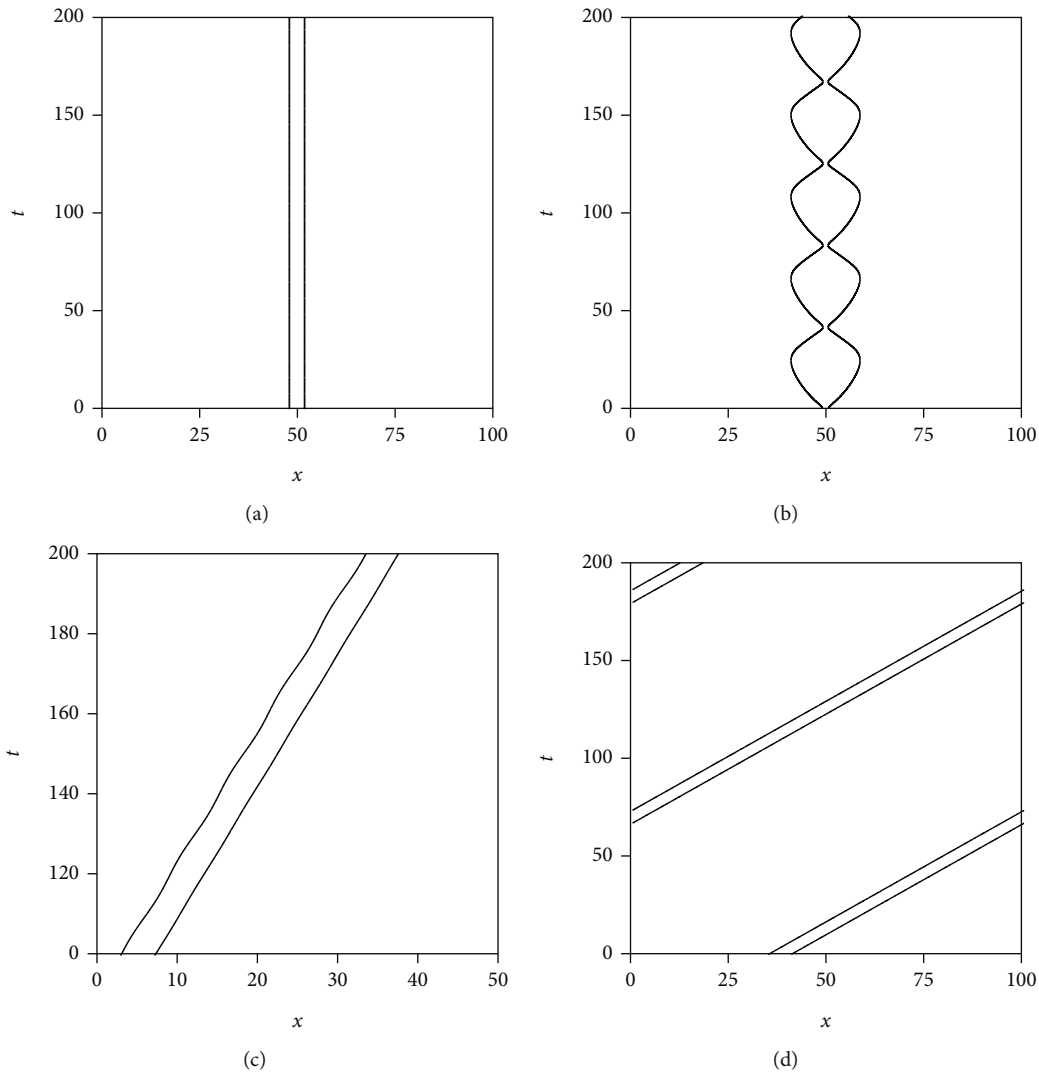

Figure 2: Four types of interface motion in the RD system (4). System size $L = 100$, $k_c = 1$, and $\theta_0 = 1 \times 10^{-2}$. (a) Standing pulse. $\tau = 0.6$. (b) Standing breather. $\tau = 0.48$. (c) Traveling breather. $\tau = 0.4743$. (d) Traveling pulse. $\tau = 0.4$. Periodic boundary condition is imposed.

$$g_3 = \frac{1}{32\left(\sqrt{D}\right)^3} + \left(\frac{2f_0k_c}{a}\right)\frac{\sqrt{2}(1-\theta_0)}{32D^2},$$
$$G_0 = \frac{1}{2} + \left(\frac{2f_0k_c}{a}\right)\frac{(1+2\theta_0)}{2\sqrt{2D}},$$
$$G_1 = \frac{1}{4\sqrt{D}} + \left(\frac{2f_0k_c}{a}\right)\frac{\sqrt{2}}{8D}, \quad (7)$$
$$\Delta_0 = \left(1 + \left(\frac{2f_0k_c}{a}\right)\frac{1}{\sqrt{2D}}\right)\theta_0.$$

The pulse width in the stationary state h_0 and the Hopf and drift bifurcation points, τ_H and τ_d, respectively, are obtained in a similar manner as that without chemotaxis by using the parameters given in Equation (7).

$$h_0 = -\sqrt{D}\log\left(\frac{\Delta_0}{G_0}\right),$$
$$\tau_H = \tau_c + \frac{1}{\sqrt{2}}\frac{\Delta_0}{G_0}\left(G_1 + \frac{G_0h_0}{2D}\right), \quad (8)$$
$$\tau_d = \tau_c - \frac{1}{\sqrt{2}}\frac{\Delta_0}{G_0}\left(G_1 + \frac{G_0h_0}{2D}\right).$$

3.2. Stability Analysis Using a Singular Perturbation Method. The stability of the standing pulse is examined by the singular perturbation method for the RD system (4) [49]. The exponential growth of the perturbation to the standing pulse solution $(h_0, \bar{v}(x))$ is determined by the roots of the equation $F_\pm(z)=0$. Here, the width $h_0=-\sqrt{D}\log(2\theta_0)$ and $\bar{v}(x)$ represents the stationary solution of the RD system (4) in the limit $\varepsilon\downarrow 0$, which is symmetric with respect to $x=0$. The brief derivation of the stability formula $F_\pm(z)$ is given in Appendix B; the final expression is

$$F_\pm(z) = -z + \frac{1}{\tau}\left(\frac{1}{\sqrt{2}} + \frac{f_0k_c(1-2\theta_0)}{\sqrt{D}a}\right) \times \left(\frac{1}{2\sqrt{D}}(1-2\theta_0) - \frac{1}{2\sqrt{D(z+1)}}\left(1 \pm e^{-h_0\sqrt{\frac{z+1}{D}}}\right)\right). \quad (9)$$

Here, F_+ and F_- correspond to the cases of symmetric and antisymmetric perturbation with respect to the center of the pulse, respectively.

$F_-(0)=0$ corresponds to the translational invariance. When $F_-(z)$ is degenerated at $z=0$, that is,

$$F_-(0) = \frac{dF_-(0)}{dz} = 0, \quad (10)$$

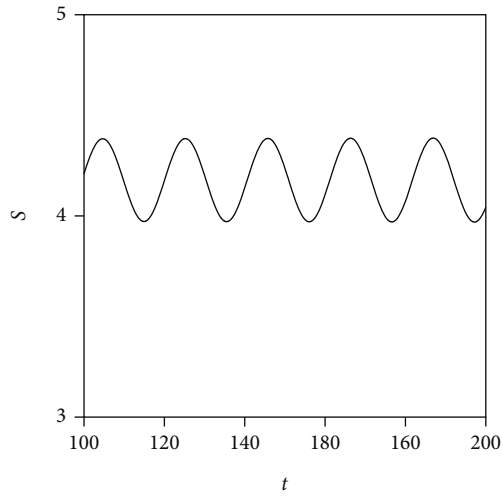

Figure 3: Oscillation of the area of traveling breather. Data are obtained by the RD system (4). $k_c=1$, $\theta_0=1\times10^{-2}$, and $\tau=0.4743$.

the standing pulse is destabilized through the translational instability; condition (10) achieves τ_d. Here, τ_d is given by

$$\tau_d = \frac{1}{4\sqrt{D}}\left(\frac{1}{\sqrt{2}} + \frac{f_0k_c(1-2\theta_0)}{\sqrt{D}a}\right)\left(1 - 2\theta_0\left(1 + \frac{h_0}{\sqrt{D}}\right)\right). \quad (11)$$

When $F_+(z)=0$ has a pair of imaginary solutions $\pm ik$ with real number k, the standing pulse is destabilized through the Hopf bifurcation; the interfaces oscillate symmetrically with respect to the center of the pulse. This condition achieves τ_H; here, τ_H is given by the solution

$$F_+(ik) = 0. \quad (12)$$

3.3. Reduced ODE System of Two Pulses. We derive the reduced ODE system of two pulses to consider the collision of two traveling pulses. We consider the case with two pulses: pulse 1 and pulse 2. Let us denote the positions of the left and right interfaces of pulse 1 as $l_1(t)$ and $l_2(t)$, respectively. Similar to pulse 1, we denote the positions of the left and right interfaces of pulse 2 as $l_3(t)$ and $l_4(t)$, respectively. We consider the nearest neighbour interaction between the interfaces. The brief derivation is given in Appendix C, and the equations of motion of l_1, l_2, l_3, and l_4 are

$$\dot{l}_1 = r_1,$$
$$\dot{l}_2 = r_2,$$
$$\dot{l}_3 = r_3,$$
$$\dot{l}_4 = r_4,$$
$$m_0\dot{r}_1 = \sqrt{2}(\tau_c - \tau)r_1 - g_3r_1^3 - (G_0 + G_1r_2)e^{-(-r_2+\phi(r_2))h/(2D)} + \Delta_0,$$

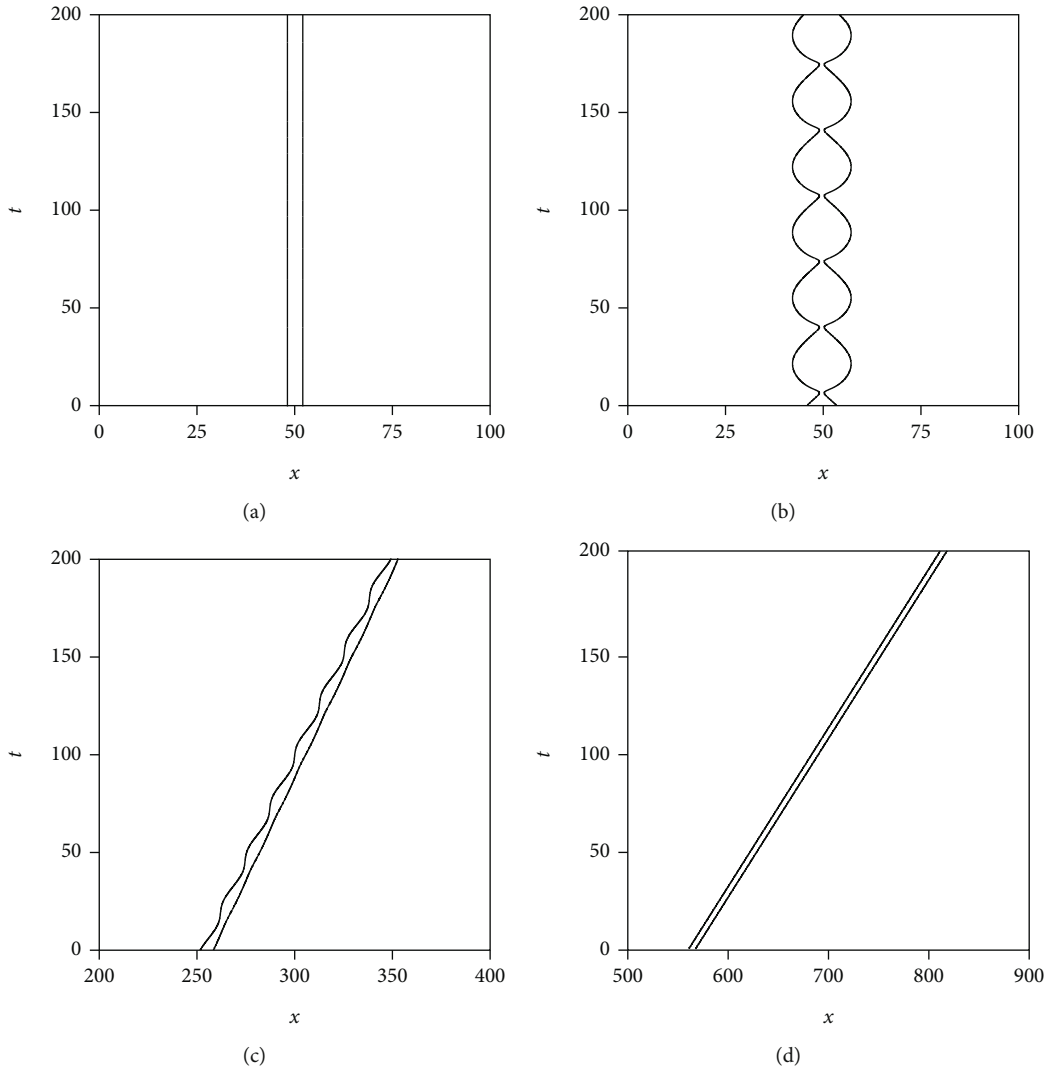

FIGURE 4: Four types of the interface motion of the reduced ODE system (6). $\theta_0 = 1 \times 10^{-2}$ and $k_c = 1$. (a) Standing pulse. $\tau = 0.7$. (b) Standing beather. $\tau = 0.55$. (c) Traveling breather. $\tau = 0.487$. (d) Traveling pulse. $\tau = 0.35$.

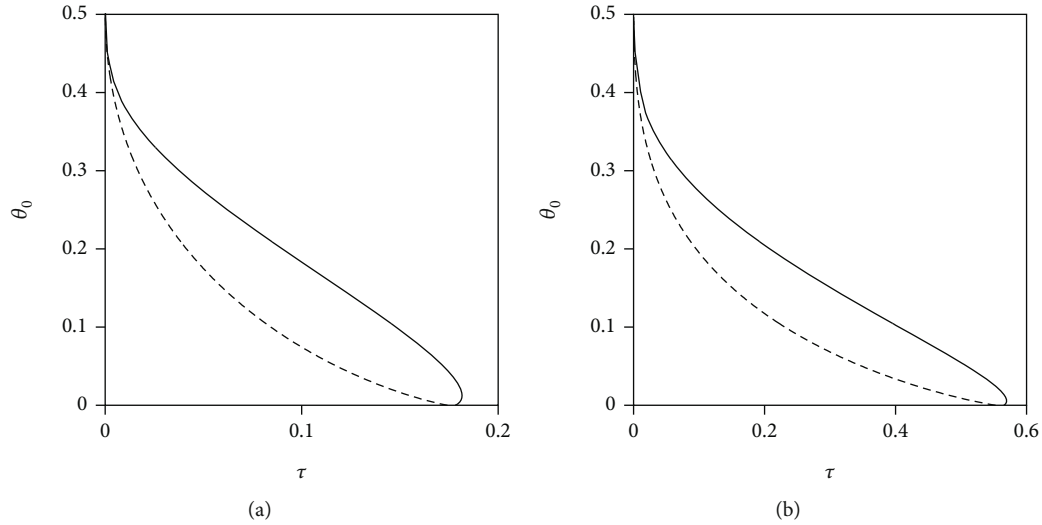

FIGURE 5: Bifurcation diagram of the standing pulse using the singular perturbation method. Solid and dashed curves represent Hopf and drift bifurcations, respectively. (a) $k_c = 0$. (b) $k_c = 1$.

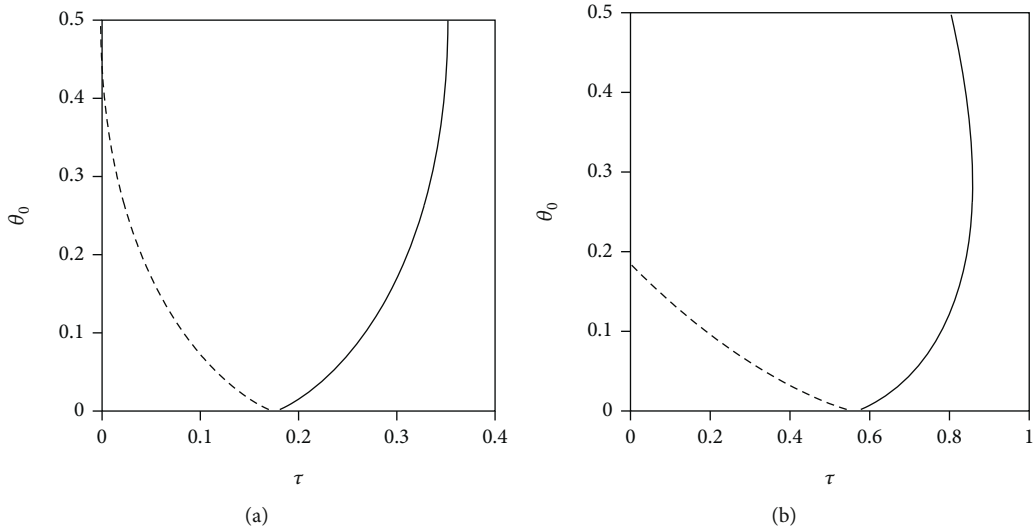

Figure 6: Bifurcation diagram of the standing pulse by the linear stability analysis for the reduced ODE system. Solid and dashed curves represent Hopf and drift bifurcations, respectively. (a) $k_c = 0$. (b) $k_c = 1$.

$$
\begin{aligned}
m_0\dot{r}_2 &= \sqrt{2}(\tau_c - \tau)r_2 - g_3 r_2^3 + (G_0 - G_1 r_1)e^{-(r_1+\phi(r_1))h/(2D)} \\
&\quad - (G_0 + G_1 r_3)e^{-(-r_3+\phi(r_3))d/(2D)} - \Delta_0, \\
m_0\dot{r}_3 &= \sqrt{2}(\tau_c - \tau)r_3 - g_3 r_3^3 - (G_0 + G_1 r_4)e^{-(-r_4+\phi(r_4))\tilde{h}/(2D)} \\
&\quad + (G_0 - G_1 r_2)e^{-(r_2+\phi(r_2))d/(2D)} + \Delta_0 \\
m_0\dot{r}_4 &= \sqrt{2}(\tau_c - \tau)r_4 - g_3 r_4^3 + (G_0 - G_1 r_3)e^{-(r_3+\phi(r_3))\tilde{h}/(2D)} \\
&\quad - \Delta_0,
\end{aligned}
\tag{13}
$$

where $h(t) = l_2(t) - l_1(t)$, $\tilde{h}(t) = l_4(t) - l_3(t)$, and $d(t) = l_3(t) - l_2(t)$ represent the pulse width of pulses 1 and 2 and the distance between the right interface of pulse 1 and the left interface of pulse 2, respectively. Parameters m_0, τ_c, g_3, G_0, G_1, and Δ_0 are the same as Equation (7). The reduced ODE system (13) is valid for $|\tau - \tau_c| \ll 1$, $0 < \theta_0 < 1/2$, $|r_i|$ $(i = 1, 2, 3, 4) \ll 1$, and $h, \tilde{h}, d \gg 1$.

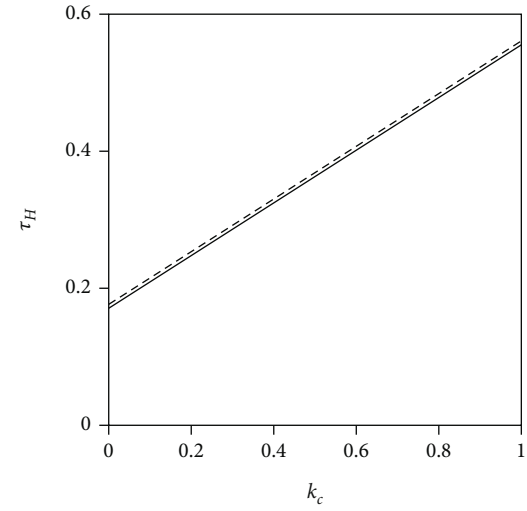

Figure 7: Dependence of the Hopf bifurcation point τ_H on k_c in the case of $\theta_0 = 1 \times 10^{-3}$. Solid and dashed curves represent data obtained using the singular perturbation method and linear analysis of the reduced ODE system, respectively.

4. Numerical Results

In this section, we consider the numerical results. In the calculation of the RD system (4), we fix $\varepsilon = 5 \times 10^{-2}$ and $D = 1$ and choose differences $\Delta x = 2.5 \times 10^{-2}$ and $\Delta t = 5 \times 10^{-4}$. The spatial direction is calculated using the implicit method under Neumann boundary conditions unless otherwise noted. Additionally, in the calculation of the reduced ODE systems (6) and (13), we employ the Runge-Kutta scheme with $\Delta t = 5 \times 10^{-4}$.

The profiles of u and v for the standing and traveling pulses in system (4) are shown in Figure 1. These profiles are almost the same with that in system (1). In the limit $\varepsilon \downarrow 0$, the profile of u becomes rectangular, connecting $u = 1/2$ with $-1/2$; the sharp edge is called the interface. For the finite value of ε $(\ll 1)$, the interface becomes a rather dull layer (inner layer), and its width is approximately $\sim \varepsilon$. By decreasing τ in system (4), four different types of solutions appear, as shown in Figure 2. Similar four types of solution are observed in system (1). Thus, solutions of the RD system Equations (4) and (1) have similar properties; the influence of chemotaxis on the solution is not evident. The area of the pulse is shown in Figure 3, where the area is defined by $S = \int_{l_1}^{l_2} dx(u(x,t) + 1/2)$; this clearly indicates the oscillation of the interface of the traveling breather ($\tau = 0.4743$). Four pulse solutions observed in the RD system (4) occur in the reduced ODE system (6), as shown in Figure 4.

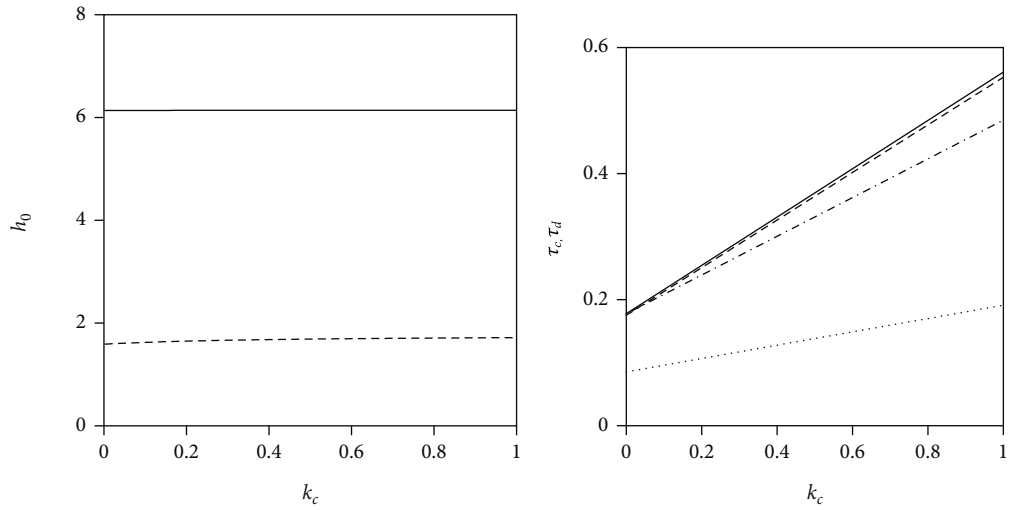

FIGURE 8: Dependence of h_0, τ_c, and τ_d on k_c. (a) Dependence of h_0 on k_c. Solid and dashed curves represent the cases $\theta_0 = 1 \times 10^{-3}$ and $\theta_0 = 1 \times 10^{-1}$, respectively. (b) Dependences of τ_c and τ_d on k_c. Solid and dashed curves represent τ_c and τ_d in the case of $\theta_0 = 1 \times 10^{-3}$, respectively. Dash-dotted and dotted curves represent τ_c and τ_d in the case of $\theta_0 = 1 \times 10^{-1}$, respectively.

These pulse solutions are also observed in the reduced ODE system (3). In our ODE system (6), the coexistence of the standing and traveling breathers are observed in a small parameter region. Thus, the reduced ODE system (6) describes similar properties observed in the RD system (4).

We consider the dependence of the Hopf and drift bifurcations on θ_0 using the singular perturbation method. Comparing Figure 5(a) with Figure 5(b), it suggests that the chemotaxis enlarges the bifurcation points; τ_d and τ_H become large under the influence of chemotaxis. To confirm the validity of the reduced ODE system (6), we calculate the bifurcation diagram using the linear stability analysis, as shown in Figure 6. When $k_c = 0$, τ_d and τ_H are symmetric with respect to $\tau \sim 0.1823$. By contrast, when $k_c = 1$, τ_d and τ_H are not symmetric. In the bifurcation diagram obtained by the singular perturbation method (Figure 5), τ_d and τ_H approach 0 with an increase in θ_0. However, when using the linear stability analysis of the reduced ODE system, τ_H does not approach 0 with an increase in θ_0. Additionally, for larger θ_0, although the Hopf bifurcation exists, the drift bifurcation does not occur. This is attributed to the fact that the amplitude of the oscillation grows larger and h becomes negative with decreasing τ; it becomes impossible to continue the calculation. Thus, τ_H obtained by the reduced ODE system is unreliable for the larger values of θ_0. For the small values of θ_0, $\tau_d \sim \tau_H$. In this case, the dependence of τ_H on k_c is calculated by two different methods: the linear stability analysis and singular perturbation method. τ_H obtained by the different methods agree well with each other, as shown in Figure 7. Thus, the reduced ODE system is reliable for small θ_0 and $|\tau - \tau_c| \ll 1$. The dependence of h_0, τ_c, and τ_d on k_c are calculated using Equations (7) and (8), as shown in Figure 8. This suggests that h_0 slightly depends on k_c, and it is almost constant. By contrast, τ_c and τ_d increase linearly with k_c. These properties hold for the small and large values of θ_0.

Let us consider the collision of two traveling pulses using the RD system (4). When the traveling velocity is low, they collide elastically; the two traveling pulses approach slowly and stop before collision with finite acceleration. Then, the pulses travel backward. By contrast, when the traveling velocity is high, the two traveling pulses collide inelastically; the two traveling pulses do not stop before collision, resulting in pair annihilation (Figure 9(a), i-ii). The parameter region of the elastic collision is shown in Figure 9(b). The parameter region of elastic collision with chemotaxis (vertically striped region) is wider than that without chemotaxis (horizontally striped region). Thus, the chemotactic substance emitted inside the pulse reduces the speed during the collision, resulting in an elastic collision. The time evolution of h and d during collision is shown in Figure 9(c), where we define the position of the interface as the position satisfying $u = 0$. Here, h and d are apparently positive; when h is locally the smallest value ($t \sim 54$), d becomes the locally maximum value, and the velocity of the two pulses becomes zero around this period.

The collision of two traveling pulses is considered using the reduced ODE system of the two pulses (13). The left and right interfaces of each pulse are traced, as shown in Figure 10(a). The interaction between the interfaces is considered among the nearest neighbours, as in Equation (13). The interface is repelled to the backward direction when an interface approaches the nearest neighbour interfaces. The pulse width h and the distance between two interfaces d can be negative under a weak repulsive force when the traveling velocity is high. In fact, when the braking effect on pulse speed is small, h and d are close to zero, as shown in Figure 10(b). The equation of motion of the interface

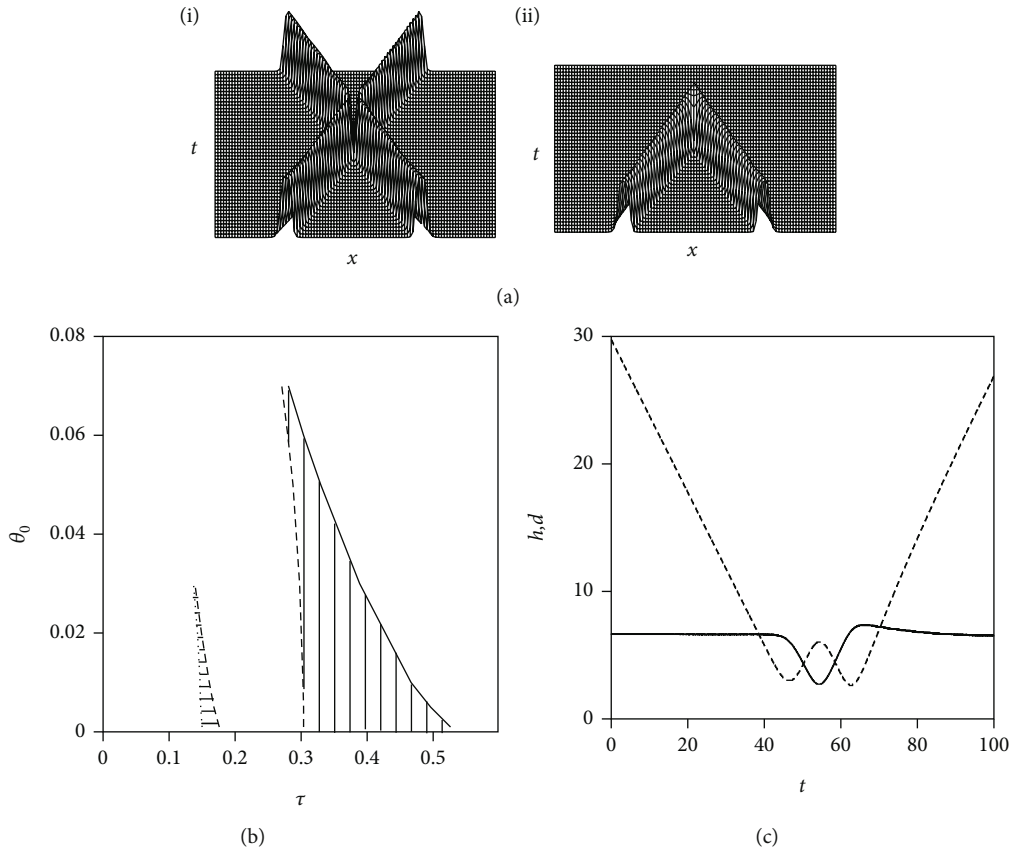

Figure 9: Collision of two traveling pulses obtained by the RD system (4). (a) Elastic collision and pair annihilation by collision. System size $L=400$, $\theta_0=1\times10^{-3}$, and $k_c=1$. (a) (i) Elastic collision. $\tau=0.51575$. (ii) Pair annihilation. $\tau=0.25157$. (b) Parameter region of elastic collision in $\tau-\theta_0$ space. Horizontally and vertically striped regions represent the parameter region, in which elastic collisions are observed in the case of $k_c=0$ and 1, respectively. (c) Time evolution of h and d. $\tau=0.51575$. Solid and dashed curves represent h and d, respectively. $\tilde{h}$=h.

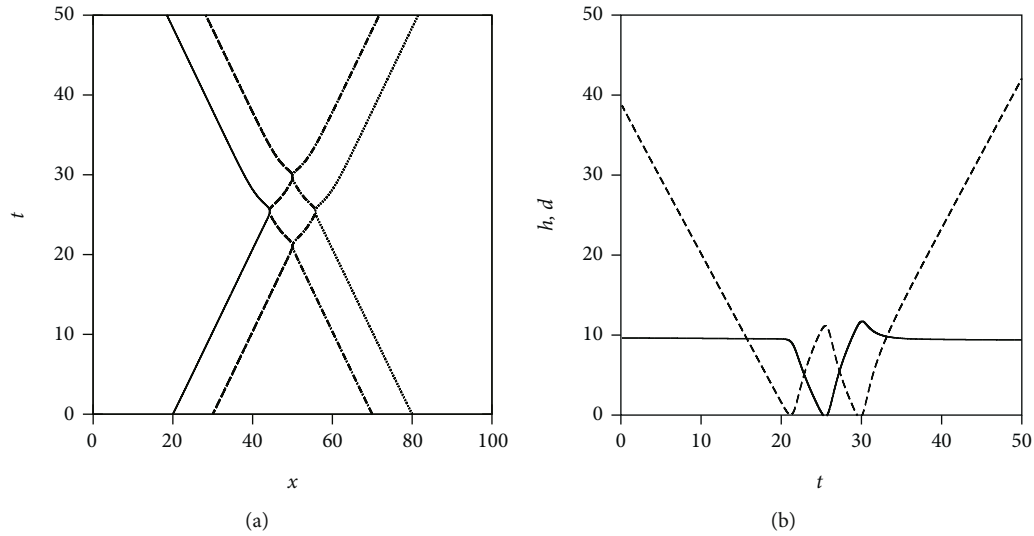

Figure 10: Collision of two traveling pulses obtained by the reduced ODE system (13). System size $L=100$, $\tau=0.45$, $\theta_0=1\times10^{-3}$, and $k_c=1$. (a) Collision of two traveling pulses. Solid, dashed, dash-dotted, and dotted curves represent l_1, l_2, l_3, and l_4, respectively. (b) Time evolution of h and d. Solid and dashed curves represent h and d, respectively. $\tilde{h}$=h.

includes a repulsive force resulted from the inhibitor (and chemotactic substance) v; therefore, the elastic collision of pulses is reasonable when the pulse velocity is low. By contrast, for a smaller τ, the pulse velocity is high, and h and d can have negative values by collision. It is impossible to calculate the time evolution for the negative values of h and d because of the divergence of exponential terms in Equation (13). Comparing Figure 10(b) with Figure 9(c), although the qualitative properties are similar, h and d become smaller in the reduced ODE system (13). For the RD system (4), with a smaller τ, the velocity of the pulse is high, and we can observe the pair annihilation of two pulses, as shown in Figure 9(a), ii. However, the reduced ODE system (13) cannot describe pair annihilation by collision.

5. Conclusions

We considered the effect of chemotaxis on pulse stability and dynamical properties. In the RD system (4), v played the dual role as a chemotactic substance and inhibitor, and influenced the motion of biological individuals. We derived the equation of motion of two interfaces, called the reduced ODE system, by applying the multiple scales method to this RD system. The equation included the linear, cubic nonlinear, and weak interacting terms and had the same form as that without chemotaxis derived in ref. [23]. The standing pulse was destabilized through the Hopf and drift bifurcations by decreasing the bifurcation parameter τ. These properties were the same as those without chemotaxis. The parameter region of the Hopf and drift bifurcations became wider under the presence of chemotaxis. To verify the validity of the reduced ODE system, we examined the stability of the standing pulse by two different methods: the singular perturbation method and linear stability of reduced ODE system. Definite differences were observed: when θ_0 was small, the reduced ODE system described the RD system well. However, for a large θ_0, the Hopf bifurcation point increased, which did not agree with the results obtained using the singular perturbation method. Thus, the reduced ODE system (6) is reliable only for $|\tau - \tau_c| \ll 1$, $0 < \theta_0 \ll 1/2$, $|r_i| \ll 1$ ($i = 1$ and 2), and $h \gg 1$.

We derived the reduced ODE system for two pulses to consider the collision of two traveling pulses. The nearest neighbour interaction was considered, and the term of repulsive force appeared in the equation that defined the motion of interfaces. Although this term decayed exponentially with the distance between the two interfaces, it caused a strong force that changed the direction of motion when the distance between the two interfaces was small. Chemotaxis enhanced the repulsive force, resulting in a wider parameter region of the elastic collision. The elastic collision of pulses with low speed was theoretically considered in an RD system without chemotaxis [19, 50–53]. The equation of motion of a pulse was derived for the pulse with low speed; this had a similar form as that of Equation (3). When the traveling velocity became zero with finite acceleration (corresponding to the third term in the left-hand side of Equation (3)), the pulse could travel in the backward direction. Although the traces of the interfaces of pulses were similar between the RD system and the reduced ODE system, the pair annihilation of pulses with a smaller τ could not be observed in the reduced ODE system. In the reduced ODE system, although the repulsive term existed, there was no restriction on the time evolution of the interfaces; this resulted in negative h, $\tilde{h}$, and d. In the RD system (4), the inhibitor (and chemotactic substance) v caused the pair annihilation of traveling pulses with high velocity. By contrast, in the reduced ODE system (13), h, $\tilde{h}$, and d could be negative, and the reduced ODE system could not describe the pair annihilation of traveling pulses with high velocity. More generally, the reduced ODE system (13) is valid under the conditions $|\tau - \tau_c| \ll 1$, $0 < \theta_0 \ll 1/2$, $|r_i| \ll 1$ ($i = 1, 2, 3, 4$), and $h, \tilde{h}, d \gg 1$. To overcome the limitation of the multiple scales method, other perturbation methods are necessary. In this study, we employed the multiple scales method to derive the reduced ODE system, and we expanded h and r using small parameters under the assumption $|\tau - \tau_d| \ll 1$. There are perturbation methods which do not require any small parameters, for example, the homotopy perturbation and variational iteration method [54–56]. Recently, He's multiple scales method was proposed, where the homotopy perturbation method was incorporated into the multiple scales method [57, 58]. Although this method is promising and may be applicable to our RD system, the discussion on detailed calculations is beyond the scope of the present study.

The collision of two traveling pulses was considered in [43]. In their model, two types of collisions were considered: an elastic collision and a fusion of two traveling pulses (inelastic collision) followed by a single traveling pulse. The concentrations of chemoattractant and nutrition were considered under the constraint of constant total bacteria. The relative strength of the attractive force caused by these two substances determined the elastic or inelastic collisions; when the attractive force caused by the chemoattractant was larger than that of the nutrition, elastic collision occurred. By contrast, when the attractive force caused by the nutrition was larger than that of chemoattractant, the fusion of two traveling pulses occurred under the constraint of constant total bacteria, followed by a single traveling pulse with the help of noise or asymmetries of the system. We note that, in their model, the pair annihilation of pulses did not appear due to the constraint of constant total bacteria. Thus, the elastic and inelastic collisions resulted from the distributions of chemoattractant and nutrition. Conversely, in our system, the chemotactic substance played the role of an inhibitor; the inhibitor in system (1) was replaced by the chemotactic substance in our system (4), and the chemotactic substance had a repulsive force on the other pulse. When the velocities of the traveling pulses were low, the repulsive force led to elastic collision. By contrast, when the velocities of the traveling pulses were high, one traveling pulse moved into the refractory zone of the other traveling pulse and resulted in the pair annihilation of the two pulses. Thus, in our system, the elastic collision and pair annihilation of traveling pulses resulted from the property of the inhibitor. In addition, the property of the chemotactic substance enlarged the parameter region of the elastic collision.

Appendix

A. Reduced ODE System of One Pulse

In this appendix, we briefly derive the reduced ODE system in the presence of chemotaxis. The equations of motion of interface are

$$\frac{dl_1}{dt} = \frac{1}{\tau}\left[\frac{v(l_1)}{\sqrt{2}} + k_c \frac{2f_0 a^3 v(l_1)}{\left(v(l_1)^2 + a^2\right)^2}\left(\frac{dv}{dx}\right)\Big|_{x=l_1}\right],$$
$$\frac{dl_2}{dt} = \frac{1}{\tau}\left[-\frac{v(l_2)}{\sqrt{2}} + k_c \frac{2f_0 a^3 v(l_2)}{\left(v(l_2)^2 + a^2\right)^2}\left(\frac{dv}{dx}\right)\Big|_{x=l_2}\right]. \tag{A.1}$$

Following ref. [23], we employ the multiple scales method to derive the equations of motion of interface. The motion of the interface is slow at the onset of the bifurcation from the standing pulse. To describe the slow motion of the interfaces, we use the scaled time $T=\mu t$, where μ is a small parameter in the range $0<\mu\ll 1$. Thus, l_i ($i=1$ and 2) and v are $l_i=l_i(T)$ as $v=v(x,T)$. Then, $v(x,T)$ is expanded with μ as

$$\begin{aligned} v(x,T) &= v_0(x,T) + \mu v_1(x,T) + \mu^2 v_2(x,T) + \mu^3 v_3(x,T) \\ &\quad + \mu^4 v_4(x,T) + \cdots \\ &= -\frac{1}{2} + \theta_0 + \bar{v}_0(x-l_2) + \mu \dot{l}_2 \bar{v}_1(x-l_2) \\ &\quad + \mu^2\left\{\ddot{l}_2 \bar{v}_{20}(x-l_2) - \dot{l}_2^2 \bar{v}_{11}(x-l_2)\right\} \\ &\quad + \mu^3\left\{\dddot{l}_2 \bar{v}_{300}(x-l_2) - \ddot{l}_2 \dot{l}_2 \bar{v}_{210}(x-l_2) \right. \\ &\quad \left. + \dot{l}_2^3 \bar{v}_{111}(x-l_2)\right\} + \cdots - \{l_1\text{terms}\}, \end{aligned} \tag{A.2}$$

where $\{l_1\text{terms}\}$ represents terms similar to the expansions of l_2 with the replacement of l_2 by l_1. Up to $O(\mu^2)$, we obtain $v(x,T)$ and $v'(x,T)$ as

$$\begin{aligned} v(x,T) &= -\frac{1}{2} + \theta_0 + \bar{U}_2^{(1)}(x-l_2) + \mu^2 \ddot{l}_2 \bar{U}_2^{(2)}(x-l_2) \\ &\quad - \bar{U}_1^{(1)}(x-l_1) - \mu^2 \ddot{l}_1 \bar{U}_1^{(2)}(x-l_1), \\ v'(x,T) &= \bar{U}_2^{(1)'}(x-l_2) + \mu^2 \ddot{l}_2 \bar{U}_2^{(2)'}(x-l_2) - \bar{U}_1^{(1)'}(x-l_1) \\ &\quad - \mu^2 \ddot{l}_1 \bar{U}_1^{(2)'}(x-l_1), \end{aligned} \tag{A.3}$$

where a prime represents the derivative of a function with respect to x, and $\bar{U}_i^{(1)}$ and $\bar{U}_i^{(2)}$ ($i=1$ and 2) are

$$\begin{aligned} &\bar{U}_i^{(1)}(x,T) \\ &= \bar{v}_0(x) + \mu \dot{l}_i \bar{v}_1(x) - \mu^2 \dot{l}_i^2 \bar{v}_{11}(x) + \mu^3 \dot{l}_i^3 \bar{v}_{111}(x) - \mu^4 \dot{l}_i^4 \bar{v}_{1111}(x) + \cdots \\ &= \begin{cases} \dfrac{1}{2} - \dfrac{\mu\dot{l}_i + \phi\left(\mu\dot{l}_i\right)}{2\phi\left(\mu\dot{l}_i\right)} \exp\left(\dfrac{-\mu\dot{l}_i + \phi\left(\mu\dot{l}_i\right)}{2D}x\right) & (x \le 0), \\ -\dfrac{1}{2} + \dfrac{-\mu\dot{l}_i + \phi\left(\mu\dot{l}_i\right)}{2\phi\left(\mu\dot{l}_i\right)} \exp\left(-\dfrac{\mu\dot{l}_i + \phi\left(\mu\dot{l}_i\right)}{2D}x\right) & (x > 0), \end{cases} \end{aligned} \tag{A.4}$$

$$\begin{aligned} &\bar{U}_i^{(2)}(x,T) \\ &= \bar{v}_{20}(x) - \mu\dot{l}_i \bar{v}_{210}(x) + \mu^2 \dot{l}_i^2 \bar{v}_{2110}(x) + \cdots \\ &= \begin{cases} \left(\dfrac{6D^2}{\phi\left(\mu\dot{l}_i\right)^5} - \dfrac{3Dx}{\phi\left(\mu\dot{l}_i\right)^4} + \dfrac{x^2}{2\phi\left(\mu\dot{l}_i\right)^3}\right) \exp\left(\dfrac{-\mu\dot{l}_i + \phi\left(\mu\dot{l}_i\right)}{2D}x\right) & (x \le 0), \\ \left(\dfrac{6D^2}{\phi\left(\mu\dot{l}_i\right)^5} + \dfrac{3Dx}{\phi\left(\mu\dot{l}_i\right)^4} + \dfrac{x^2}{2\phi\left(\mu\dot{l}_i\right)^3}\right) \exp\left(-\dfrac{\mu\dot{l}_i + \phi\left(\mu\dot{l}_i\right)}{2D}x\right) & (x > 0), \end{cases} \end{aligned} \tag{A.5}$$

where $\phi(r)=\sqrt{4D+r^2}$. The first term of (A.1) is already estimated in ref. [23]. We show the final result of the second term, which is the chemotaxis term. Let us consider the equation of motion of l_2. When $\dot{l}_2$ is small, the denominator $\left(v(l_2)^2 + a^2\right)^2$ can be approximated as a^4. Using expressions of $\bar{U}_i^{(1,2)}$, we obtain

$$\begin{aligned} v(l_2) &\sim \mu\dot{l}_2\left(-\frac{1}{4\sqrt{D}} + \frac{\mu^2}{32D^{3/2}}\dot{l}_2^2\right) + \theta_0 \\ &\quad + \left(-\frac{1}{2} + \frac{\mu}{4\sqrt{D}}\dot{l}_1\right) e^{-\left(\mu\dot{l}_1 + \phi\left(\mu\dot{l}_1\right)\right)h/(2D)} \\ &\quad + \frac{3\mu^2}{16\sqrt{D}}\ddot{l}_2, \\ v(l_2)\left(\frac{dv}{dx}\right)\Big|_{x=l_2} &\sim \mu\dot{l}_2\left(\frac{1}{8D}(1-2\theta_0) - \frac{\mu^2}{32D^2}(1-\theta_0)\dot{l}_2^2\right) \\ &\quad - \frac{1}{\sqrt{4D}}\theta_0 + \left(\frac{1}{2\sqrt{4D}}(1+2\theta_0) - \frac{\mu}{8D}\dot{l}_1\right) \\ &\quad \cdot e^{-\left(\mu\dot{l}_1 + \phi\left(\mu\dot{l}_1\right)\right)h/(2D)} - \frac{3\mu^2}{32D}\ddot{l}_2. \end{aligned} \tag{A.6}$$

Substituting the above equations into the second term of (A.1) and putting $\mu=1$, we can derive the equation of motion of l_2. Similarly, we can derive the equation of motion of l_1; the final expressions of the equation of motion of the interfaces are given in (6) with the parameters given in (7).

B. Stability Formula Using a Singular Perturbation Method

In this appendix, following the singular perturbation method [49], we briefly derive the stability formula $F_\pm$ given in Section 3. Let us consider the symmetric solution with respect to $x=0$, which is denoted by $(h_0, \bar{v}(x))$, where the

pulse width $h_0=-\sqrt{D}\log(2\theta_0)$ and $\bar{v}(x)$ is a stationary solution of (4) in the limit $\varepsilon\downarrow 0$.

The velocity of the pulse is given (for derivation, see refs. [31, 36, 47]) by

$$C\left(v,v'\right)=\frac{1}{\tau}\left[\frac{v(x)}{\sqrt{2}}+k_c\frac{2f_0a^3v(x)}{\left(v(x)^2+a^2\right)^2}\left(\frac{dv}{dx}\right)\right], \tag{B.1}$$

where v' represents (dv/dx). The perturbations are supplied to the stationary solution, and we assume that the left and right interface positions are shifted as $l_1(t)=-h_0/2+\xi_1(t)$ and $l_2(t)=h_0/2+\xi_2(t)$, respectively. Using (B.1), the velocities at the left front $x=l_1$ and right front l_2 are given by

$$\begin{aligned}\frac{dl_1}{dt}&=\frac{1}{\tau}\left[\frac{v(l_1)}{\sqrt{2}}+k_c\frac{2f_0a^3v(l_1)}{\left(v(l_1)^2+a^2\right)^2}\left(\frac{dv}{dx}\right)\Bigg|_{x=l_1}\right],\\ \frac{dl_2}{dt}&=\frac{1}{\tau}\left[-\frac{v(l_2)}{\sqrt{2}}+k_c\frac{2f_0a^3v(l_2)}{\left(v(l_2)^2+a^2\right)^2}\left(\frac{dv}{dx}\right)\Bigg|_{x=l_2}\right],\end{aligned} \tag{B.2}$$

respectively. We expand $v(x)$ and $v'(x)$ around the interface position, such that $v=v_0+v_1(t)+v_2(t)$ and $v'=v'_0+v'_1(t)+v'_2(t)$, respectively. The velocity $C(v,v')$ is expanded around (v_0,v_0'), where $C(v_0,v_0')=0$ is satisfied, as

$$C\left(v,v'\right)=C\left(v_0,v_0'\right)+\frac{\partial C}{\partial v}\Big|_0\left(v_1+v_2\right)+\frac{\partial C}{\partial v'}\Big|_0\left(v'_1+v'_2\right), \tag{B.3}$$

where $A|_0$ represents A evaluated at $x=\pm h_0/2$. After several calculations, we obtain

$$\begin{aligned}v_0(\pm h_0/2)&=0,\\ v_1(-h_0/2+\xi_1)&=\frac{(1-2\theta_0)}{2\sqrt{D}}\xi_1,\quad v_1(h_0/2+\xi_2)=-\frac{(1-2\theta_0)}{2\sqrt{D}}\xi_2,\\ v_2(-h_0/2+\xi_1)&=\frac{1}{2\pi}\int dq\int_0^t dt'\,D_q^{(1)}\left(t-t'\right)e^{-\left(Dq^2+1\right)t'-iqh_0/2},\\ v_2(h_0/2+\xi_2)&=\frac{1}{2\pi}\int dq\int_0^t dt'\,D_q^{(1)}\left(t-t'\right)e^{-\left(Dq^2+1\right)t'+iqh_0/2},\\ v'_0(\pm h_0/2)&=\mp\frac{(1-2\theta_0)}{2\sqrt{D}},\\ v'_1(-h_0/2+\xi_1)&=\frac{-\theta_0}{D}\xi_1,\quad v'_1(h_0/2+\xi_2)=\frac{-\theta_0}{D}\xi_2,\\ v'_2(-h_0/2+\xi_1)&=\frac{i}{2\pi}\int dq\int_0^t dt'\,qD_q^{(1)}\left(t-t'\right)e^{-\left(Dq^2+1\right)t'-iqh_0/2},\\ v'_2(h_0/2+\xi_2)&=\frac{i}{2\pi}\int dq\int_0^t dt'\,qD_q^{(1)}\left(t-t'\right)e^{-\left(Dq^2+1\right)t'+iqh_0/2},\end{aligned} \tag{B.4}$$

where $D_q^{(1)}$ is given by

$$D_q^{(1)}\left(t-t'\right)=-\left(e^{iqh_0/2}\xi_1\left(t-t'\right)-e^{-iqh_0/2}\xi_2\left(t-t'\right)\right). \tag{B.5}$$

To express (B.2) in a linear form in terms of ξ_1 and ξ_2, we define the Laplace transformation of $\xi(t)$ as

$$\widehat{\xi}(z)=\int_0^\infty\xi(t)e^{-zt}dt. \tag{B.6}$$

Using

$$\begin{aligned}\frac{\partial C}{\partial v}\Big|_{x=\pm h_0/2}&=\mp\frac{1}{\tau}\left(\frac{1}{\sqrt{2}}+\frac{f_0k_c(1-2\theta_0)}{\sqrt{D}a}\right),\\ \frac{\partial C}{\partial v'}\Big|_{x=\pm h_0/2}&=0,\end{aligned} \tag{B.7}$$

we apply the Laplace transformation to (B.2) to obtain

$$\begin{aligned}-\xi(0)&=\left[-z+\frac{1}{\tau}\left(\frac{1}{\sqrt{2}}+\frac{f_0k_c(1-2\theta_0)}{\sqrt{D}a}\right)\right.\\ &\quad\left.\times\left(\frac{1}{2\sqrt{D}}(1-2\theta_0)-\frac{1}{2\sqrt{D(z+1)}}\left(1\pm e^{-h_0\sqrt{\frac{z+1}{D}}}\right)\right)\right]\widehat{\xi}(z)\\ &\equiv F_\pm(z)\widehat{\xi}(z),\end{aligned} \tag{B.8}$$

where we considered the two modes of perturbation: the symmetric perturbation with respect to the center of the pulse $-\xi_1=\xi_2=\xi$ and the antisymmetric perturbation $\xi_1=\xi_2=\xi$. F_+ and F_- correspond to the symmetric and antisymmetric case, respectively.

C. Reduced ODE System of Two Pulses

In this appendix, we briefly show the derivation of the interacting term in the reduced ODE system of two pulses in the presence of chemotaxis. We assume that the interaction among the interfaces occurs between the nearest neighbours. Then, the interaction term between two pulses appears in the equations of motion of l_2 and l_3, and the interaction decays exponentially with distance $d=l_3-l_2$; this is valid for $d\gg D$.

Following ref. [23], we introduce a small parameter μ $(0<\mu\ll 1)$ to employ the multiple scales method.

Using μ, we introduce a slow time scale $T=\mu t$. Then, $v(x,T)$ is expanded as

$$\begin{aligned} v(x,T) &= v_0(x,T) + \mu v_1(x,T) + \mu^2 v_2(x,T) + \mu^3 v_3(x,T) \\ &\quad + \mu^4 v_4(x,T) + \cdots \\ &= -\frac{1}{2} + \theta_0 + \bar{v}_0(x-l_2) + \mu \dot{l}_2 \bar{v}_1(x-l_2) \\ &\quad + \mu^2 \left\{ \ddot{l}_2 \bar{v}_{20}(x-l_2) - \dot{l}_2^2 \bar{v}_{11}(x-l_2) \right\} \\ &\quad + \mu^3 \left\{ \dddot{l}_2 \bar{v}_{300}(x-l_2) - \ddot{l}_2 \dot{l}_2 \bar{v}_{210}(x-l_2) + \dot{l}_2^3 \bar{v}_{111}(x-l_2) \right\} \\ &\quad + \cdots - \{l_1\text{terms}\} + \{l_4\text{terms}\} - \{l_3\text{terms}\}, \end{aligned} \tag{C.1}$$

where $l_i=l_i(T)$ ($i=1,2,\cdots,4$) and $\{l_1(l_4,l_3)\text{terms}\}$ represent the terms similar to expansions of l_2 with the replacement of l_2 by $l_1(l_4,l_3)$. Let us consider the equation of motion of l_2. We include terms up to $O(\mu^3)$, and we substitute $v(x,T)$ and $v'(x,T)$ into the equation of motion of the interface such as

$$\frac{dl_2}{dt} = \frac{1}{\tau}\left[-\frac{v(l_2)}{\sqrt{2}} + k_c \frac{2f_0 a^3 v(l_2)}{\left(v(l_2)^2 + a^2\right)^2} \left(\frac{dv}{dx}\right)\Big|_{x=l_2} \right]. \tag{C.2}$$

Up to $O(\mu^2)$, we obtain the approximation of $v(x,T)$ as

$$\begin{aligned} v(x,T) &= -\frac{1}{2} + \theta_0 + \bar{U}_2^{(1)}(x-l_2) + \mu^2 \ddot{l}_2 \bar{U}_2^{(2)}(x-l_2) \\ &\quad - \bar{U}_1^{(1)}(x-l_1) - \mu^2 \ddot{l}_1 \bar{U}_1^{(2)}(x-l_1) + \bar{U}_4^{(1)}(x-l_4) \\ &\quad + \mu^2 \ddot{l}_4 \bar{U}_4^{(2)}(x-l_4) - \bar{U}_3^{(1)}(x-l_3) - \mu^2 \ddot{l}_3 \bar{U}_3^{(2)}(x-l_3), \end{aligned} \tag{C.3}$$

where $\bar{U}_i^{(1)}$ and $\bar{U}_i^{(2)}$ ($i=1,2,\cdots,4$) are the same as (A.4) and (A.5). Using (C.3),

$$\begin{aligned} v(l_2) &= -\frac{1}{2} + \theta_0 + \bar{U}_2^{(1)}(0) + \mu^2 \ddot{l}_2 \bar{U}_2^{(2)}(0) - \bar{U}_1^{(1)}(h) \\ &\quad - \mu^2 \ddot{l}_1 \bar{U}_1^{(2)}(h) + \bar{U}_4^{(1)}\left(-d-\tilde{h}\right) + \mu^2 \ddot{l}_4 \bar{U}_4^{(2)}\left(-d-\tilde{h}\right) \\ &\quad - \bar{U}_3^{(1)}(-d) - \mu^2 \ddot{l}_3 \bar{U}_3^{(2)}(-d). \end{aligned} \tag{C.4}$$

As we consider the nearest neighbour interaction, terms $\bar{U}_4^{(1,2)}(-d-\tilde{h})$ can be neglected in (C.4). Similarly, we can derive $v(l_3)$ as

$$\begin{aligned} v(l_3) &= -\frac{1}{2} + \theta_0 + \bar{U}_2^{(1)}(d) + \mu^2 \ddot{l}_2 \bar{U}_2^{(2)}(d) - \bar{U}_1^{(1)}(h+d) \\ &\quad - \mu^2 \ddot{l}_1 \bar{U}_1^{(2)}(h+d) + \bar{U}_4^{(1)}\left(-\tilde{h}\right) + \mu^2 \ddot{l}_4 \bar{U}_4^{(2)}\left(-\tilde{h}\right) \\ &\quad - \bar{U}_3^{(1)}(0) - \mu^2 \ddot{l}_3 \bar{U}_3^{(2)}(0), \end{aligned} \tag{C.5}$$

where terms $\bar{U}_1^{(1,2)}(h+d)$ can be neglected in (C.5). Under our assumption, there is no term accompanying d in the expressions of $v(l_1)$ and $v(l_4)$. This indicates that the equations of motion of l_1 and l_4 are a similar form to those of l_1 and l_2 in (6), respectively. Substituting $v(l_i)$ into the equation of motion of each interface under the above considerations and putting $\mu=1$, we can derive the equations of motion of l_i as indicated in (13).

Data Availability

The data that support the findings of this study are included in the article.

Conflicts of Interest

The author declares that there are no conflicts of interest.

References

[1] I. M. Sokolov and J. Klafter, "From diffusion to anomalous diffusion: a century after Einstein's Brownian motion," *Chaos*, vol. 15, no. 2, Article ID 026103, 2005.

[2] A. S. Chaves, "A fractional diffusion equation to describe Lévy flights," *Physics Letters A*, vol. 239, no. 1-2, pp. 13–16, 1998.

[3] R. Metzler and J. Klafter, "The random walk's guide to anomalous diffusion: a fractional dynamics approach," *Physics Reports*, vol. 339, no. 1, pp. 1–77, 2000.

[4] W. Chen, "Time-space fabric underlying anomalous diffusion," *Chaos, Solitons and Fractals*, vol. 28, no. 4, pp. 923–929, 2006.

[5] W. Chen, H. Sun, X. Zhang, and D. Korošak, "Anomalous diffusion modeling by fractal and fractional derivatives," *Computers and Mathematics with Applications*, vol. 59, no. 5, pp. 1754–1758, 2010.

[6] Y. Wu, "Variational approach to fractal reaction-diffusion equations with fractal derivatives," *Thermal Science*, vol. 25, no. 2B, pp. 1425–1430, 2021.

[7] I. Ateş and P. A. Zegeling, "A homotopy perturbation method for fractional-order advection-diffusion- reaction boundary-value problems," *Applied Mathematical Modelling*, vol. 47, pp. 425–441, 2017.

[8] Y. Wang, M. Du, F. Tan, Z. Li, and T. Nie, "Using reproducing kernel for solving a class of fractional partial differential equation with non-classical conditions," *Applied Mathematics and Computation*, vol. 219, no. 11, pp. 5918–5925, 2013.

[9] A. W. Liehr, *Dissipative Solitons in Reaction Diffusion Systems: Mechanisms, Dynamics, Interaction*, Springer-Verlag, Berlin, 2013.

[10] V. K. Vanag, "Waves and patterns in reaction-diffusion systems. Belousov-Zhabotinsky reaction in water-in-oil microemulsions," *Physics-Uspekhi*, vol. 47, no. 9, pp. 923–941, 2004.

[11] N. F. Britton, *Reaction-Diffusion Equations and their Applications to Biology*, Elsevier Academic Press, London, 1986.

[12] J. Lefèvre and J.-F. Mangin, "A reaction-diffusion model of human brain development," *Plos Computational Biology*, vol. 6, no. 4, article e1000749, 2010.

[13] A. M. Turing, "The chemical basis of morphogenesis," *Philosophical Transactions of the Royal Society of London. Series B, Biological Sciences*, vol. 237, no. 641, pp. 37–72, 1952.

[14] K. Kawasaki and T. Ohta, "Kink dynamics in one-dimensional nonlinear systems," *Physica A: Statistical Mechanics and its Applications*, vol. 116, no. 3, pp. 573–593, 1982.

[15] C. M. Elliot, "The Cahn-Hilliard model for the kinetics of phase separation," in *Mathematical Models for Phase Change Problems*, J. F. Rodrigues, Ed., vol. 88, pp. 35–73, Birkhäuser-Verlag, Basel, Switzerland, 1989.

[16] S.-I. Ei and T. Ohta, "Equation of motion for interacting pulses," *Physical Review E: Statistical, Nonlinear, Biological, and Soft Matter Physics*, vol. 50, no. 6, pp. 4672–4678, 1994.

[17] T. Ogawa and C. Liu, "Two-dimensional patterns of pulses appearing in a thin viscous film flow," *Physica D: Nonlinear Phenomena*, vol. 108, no. 3, pp. 277–290, 1997.

[18] S.-I. Ei, "The motion of weakly interacting pulses in reaction-diffusion systems," *Journal of Dynamics and Differential Equations*, vol. 14, no. 1, pp. 85–137, 2002.

[19] S.-I. Ei, M. Mimura, and M. Nagayama, "Pulse-pulse interaction in reaction-diffusion systems," *Physica D: Nonlinear Phenomena*, vol. 165, no. 3-4, pp. 176–198, 2002.

[20] S.-I. Ei, H. Ikeda, and T. Kawana, "Dynamics of front solutions in a specific reaction-diffusion system in one dimension," *Japan Journal of Industrial and Applied Mathematics*, vol. 25, no. 1, pp. 117–147, 2008.

[21] K. Nishi, Y. Nishiura, and T. Teramoto, "Dynamics of two interfaces in a hybrid system with jump-type heterogeneity," *Japan Journal of Industrial and Applied Mathematics*, vol. 30, no. 2, pp. 351–395, 2013.

[22] T. Kusaka, *Master's thesis, in Japanese*, Kyushu University, Japan, 2007.

[23] K. Nishi, Y. Nishiura, and T. Teramoto, "Reduction approach to the dynamics of interacting front solutions in a bistable reaction-diffusion system and its application to heterogeneous media," *Physica D: Nonlinear Phenomena*, vol. 398, pp. 183–207, 2019.

[24] A. Hagberg, E. Meron, I. Rubinstein, and B. Zaltzman, "Controlling domain patterns far from equilibrium," *Physical Review Letters*, vol. 76, no. 3, pp. 427–430, 1996.

[25] A. Hagberg, E. Meron, I. Rubinstein, and B. Zaltzman, "Order parameter equations for front transitions: planar and circular fronts," *Physical Review E: Statistical, Nonlinear, Biological, and Soft Matter Physics*, vol. 55, no. 4, pp. 4450–4457, 1997.

[26] P. Krämer, "The method of multiple scales for nonlinear Klein-Gordon and Schrödinger equations," *Ph. D. Thesis*, Karlsruhe Institute of Technology, Karlsruhe, Germany, 2013.

[27] M. P. Brenner, L. S. Levitov, and E. O. Budrene, "Physical mechanisms for chemotactic pattern formation by bacteria," *Biophysical Journal*, vol. 74, no. 4, pp. 1677–1693, 1998.

[28] M. Seyrich, "Statistical physics of bacterial chemotaxis," *Ph. D. Thesis*, Technische Universität Berlin, Berlin, Germany, 2020.

[29] J. Adler, "Chemotaxis in bacteria: Motile *Escherichia coli* migrate in bands that are influenced by oxygen and organic nutrients," *Science*, vol. 153, no. 3737, pp. 708–716, 1966.

[30] J. D. Murray, *Mathematical Biology*, Springer-Verlag, Berlin, 3rd edition, 2002.

[31] S. Kawaguchi, "Motion of a spot in a reaction diffusion system under the influence of chemotaxis," *Advances in Mathematical Physics*, vol. 2018, Article ID 6152961, 24 pages, 2018.

[32] M. Seyrich, A. Palugniok, and H. Stark, "Traveling concentration pulses of bacteria in a generalized Keller-Segel model," *New Journal of Physics*, vol. 21, no. 10, article 103001, 2019.

[33] E. F. Keller and L. A. Segel, "Initiation of slime mold aggregation viewed as an instability," *Journal of Theoretical Biology*, vol. 26, no. 3, pp. 399–415, 1970.

[34] E. F. Keller and L. A. Segel, "Traveling bands of chemotactic bacteria: a theoretical analysis," *Journal of Theoretical Biology*, vol. 30, no. 2, pp. 235–248, 1971.

[35] R. Erban and H. G. Othmer, "From individual to collective behavior in bacterial chemotaxis," *SIAM Journal on Applied Mathematics*, vol. 65, no. 2, pp. 361–391, 2004.

[36] S. Kawaguchi, "Chemotaxis-growth under the influence of lateral inhibition in a three-component reaction-diffusion system," *Nonlinearity*, vol. 24, no. 4, pp. 1011–1031, 2011.

[37] S. Saha, R. Golestanian, and S. Ramaswamy, "Clusters, asters, and collective oscillations in chemotactic colloids," *Physical Review E: Statistical, Nonlinear, Biological, and Soft Matter Physics*, vol. 89, no. 6, Article ID 062316, 2014.

[38] Z. Du, J. Liu, and Y. Ren, "Traveling pulse solutions of a generalized Keller-Segel system with small cell diffusion via a geometric approach," *Journal of Differential Equations*, vol. 270, pp. 1019–1042, 2021.

[39] Y. Li, Y. Li, Y. Wu, and H. Zhang, "Spectral stability of bacteria pulses for a Keller-Segel chemotactic model," *Journal of Differential Equations*, vol. 304, pp. 229–286, 2021.

[40] J. Saragosti, V. Calvez, N. Bournaveas, A. Buguin, P. Silberzan, and B. Perthame, "Mathematical description of bacterial traveling pulses," *PLoS Computational Biology*, vol. 6, no. 8, article e1000890, 2010.

[41] C. Emako, C. Gayrard, A. Buguin, L. N. de Almeida, and N. Vauchelet, "Traveling pulses for a two-species chemotaxis model," *PLoS Computational Biology*, vol. 12, no. 4, article e1004843, 2016.

[42] A. V. Narla, J. Cremer, and T. Hwa, "A traveling-wave solution for bacterial chemotaxis with growth," *Proceedings of the National Academy of Sciences*, vol. 118, no. 48, article e2105138118, 2021.

[43] G. Young, M. Demir, H. Salman, G. B. Ermentrout, and J. E. Rubin, "Interactions of solitary pulses of *E. coli* in a one-dimensional nutrient gradient," *Physica D: Nonlinear Phenomena*, vol. 395, pp. 24–36, 2019.

[44] T. Nagai and T. Ikeda, "Traveling waves in a chemotactic model," *Journal of Mathematical Biology*, vol. 30, no. 2, pp. 169–184, 1991.

[45] D. Horstmann and A. Stevens, "A constructive approach to traveling waves in chemotaxis," *Journal of Nonlinear Science*, vol. 14, no. 1, pp. 1–25, 2004.

[46] H. Izuhara, K. Kuto, and T. Tsujikawa, "Bifurcation structure of stationary solutions for a chemotaxis system with bistable growth," *Japan Journal of Industrial and Applied Mathematics*, vol. 35, no. 2, pp. 441–475, 2018.

[47] J. Rinzel and D. Terman, "Propagation phenomena in a bistable reaction-diffusion system," *SIAM Journal on Applied Mathematics*, vol. 42, no. 5, pp. 1111–1137, 1982.

[48] M. Mimura and T. Tsujikawa, "Aggregating pattern dynamics in a chemotaxis model including growth," *Physica A: Statistical Mechanics and its Applications*, vol. 230, no. 3-4, pp. 499–543, 1996.

[49] T. Ohta, M. Mimura, and R. Kobayashi, "Higher-dimensional localized patterns in excitable media," *Physica D: Nonlinear Phenomena*, vol. 34, no. 1-2, pp. 115–144, 1989.

[50] T. Ohta, J. Kiyose, and M. Mimura, "Collision of propagating pulses in a reaction-diffusion system," *Journal of the Physical Society of Japan*, vol. 66, no. 5, pp. 1551–1558, 1997.

[51] T. Ohta, "Pulse dynamics in a reaction-diffusion system," *Physica D: Nonlinear Phenomena*, vol. 151, no. 1, pp. 61–72, 2001.

[52] M. Mimura, M. Nagayama, and T. Ohta, "Non-annihilation of travelling pulses in a reaction-diffusion system," *Methods and Applications of Analysis*, vol. 9, no. 4, pp. 493–516, 2002.

[53] T. Teramoto, K.-I. Ueda, and Y. Nishiura, "Phase-dependent output of scattering process for traveling breathers," *Physical Review E: Statistical, Nonlinear, Biological, and Soft Matter Physics*, vol. 69, no. 5, Article ID 056224, 2004.

[54] J.-H. He, "Homotopy perturbation technique," *Computer Methods in Applied Mechanics and Engineering*, vol. 178, no. 3-4, pp. 257–262, 1999.

[55] J.-H. He, "Variational iteration method - a kind of non-linear analytical technique: some examples," *International Journal of Non-Linear Mechanics*, vol. 34, no. 4, pp. 699–708, 1999.

[56] S. Chakraverty, N. R. Mahato, P. Karunakar, and T. D. Rao, *Advanced Numerical and Semi-Analytical Methods for Differential Equations*, Wiley, New York, 2019.

[57] Y. O. El-Dib, "Periodic solution and stability behavior for nonlinear oscillator having a cubic nonlinearity time-delayed," *International Annals of Science*, vol. 5, no. 1, pp. 12–25, 2018.

[58] Y. O. El-Dib, "Periodic solution of the cubic nonlinear Klein-Gordon equation and the stability criteria via the He-multiple-scales method," *Pramana - Journal of Physics*, vol. 92, no. 1, Article ID 7, 2019.